Nuclear Instruments and Methods in Physics Research A 1076 (2025) 170467

Contents lists available at ScienceDirect

Nuclear Inst. and Methods in Physics Research, A

journal homepage: www.elsevier.com/locate/nima

CMS RPC performance and operation in LHC Run 3

M. Shopova [5,*], M. Tytgat [1,a], K. Mota Amarilo [2,b], A. Samalan [2,c], K. Skovpen [2], G.A. Alves [3], E. Alves Coelho [3], F. Marujo da Silva [3], M. Barroso Ferreira Filho [4], E.M. Da Costa [4], D. De Jesus Damiao [4], S. Fonseca De Souza [4], R. Gomes De Souza [4], L. Mundim [4], H. Nogima [4], J.P. Pinheiro [4], A. Santoro [4], M. Thiel [4], A. Aleksandrov [5], R. Hadjiiska [5], P. Iaydjiev [5], G. Sultanov [5], A. Dimitrov [6], L. Litov [6], B. Pavlov [6], P. Petkov [6], A. Petrov [6], E. Shumka [6], P. Cao [7], W. Diao [7], Q. Hou [7], H. Kou [7], Z.-A. Liu [7], J. Song [7], J. Zhao [7], S.J. Qian [8], C. Avila [9], D.A. Barbosa Trujillo [9], A. Cabrera [9], C.A. Florez [9], J.A. Reyes Vega [9], R. Aly [10,12,d], A. Radi [11,e], Y. Assran [12,f], I. Crotty [13], M.A. Mahmoud [13], M. Gouzevitch [14], G. Grenier [14], I.B. Laktineh [14], L. Mirabito [14], I. Bagaturia [15], I. Lomidze [15], Z. Tsamalaidze [15,g], V. Amoozegar [16], B. Boghrati [16], M. Ebrahimi [16], F. Esfandi [16], Y. Hosseini [16], M. Mohammadi Najafabadi [16], E. Zareian [16], M. Abbrescia [17,18], N. De Filippis [17,19], G. Iaselli [17,19], F. Loddo [17], G. Pugliese [17,19], D. Ramos [17], L. Benussi [20], S. Bianco [20], S. Meola [20,h], D. Piccolo [20], S. Buontempo [21], F. Carnevali [21,22], L. Lista [21,22,i], P. Paolucci [21,j], F. Fienga [23], A. Braghieri [24], P. Montagna [24,25], C. Riccardi [24,25], P. Salvini [24], P. Vitulo [24,25], E. Asilar [26], T.J. Kim [26], Y. Ryou [26], S. Choi [27], B. Hong [27], K.S. Lee [27], J. Goh [28], J. Shin [28], Y. Lee [29], I. Pedraza [30], C. Uribe Estrada [30], H. Castilla-Valdez [31], R. Lopez-Fernandez [31], A. Sánchez Hernández [31], M. Ramírez García [32], D.L. Ramirez Guadarrama [32], M.A. Shah [32], E. Vazquez [32], N. Zaganidis [32], A. Ahmad [33], M.I. Asghar [33], H.R. Hoorani [33], S. Muhammad [33], J. Eysermans [34], on behalf of the CMS Collaboration

[1] *Vrije Universiteit Brussel, Brussel, Belgium*
[2] *Universiteit Gent, Gent, Belgium*
[3] *Centro Brasileiro de Pesquisas Fisicas, Rio de Janeiro, Brazil*
[4] *Universidade do Estado do Rio de Janeiro, Rio de Janeiro, Brazil*
[5] *Institute for Nuclear Research and Nuclear Energy, Bulgarian Academy of Sciences, Sofia, Bulgaria*
[6] *Faculty of Physics, University of Sofia, Sofia, Bulgaria*
[7] *Institute of High Energy Physics and University of the Chinese Academy of Sciences, Beijing, China*
[8] *School of Physics, Peking University, Beijing, China*
[9] *Universidad de Los Andes, Bogota, Colombia*
[10] *Physics Department, Faculty of science, Helwan University, Cairo, Egypt*

* Corresponding author.
E-mail address: mariana.vutova@cern.ch (M. Shopova).
[a] Also at Ghent University, Ghent, Belgium.
[b] Now at UERJ, Rio de Janeiro, Brazil.
[c] Now at PSI, Villigen, Switzerland.
[d] Also at Academy of Scientific Research and Technology of the Arab Republic of Egypt, Egyptian Network of High Energy Physics, Cairo, Egypt.
[e] Also at Sultan Qaboos University, Muscat, Oman.
[f] Also at Suez University, Suez, Egypt.
[g] Also at an institute or an international laboratory covered by a cooperation agreement with CERN.
[h] Also at Università degli Studi Guglielmo Marconi, Roma, Italy.
[i] Also at Scuola Superiore Meridionale, Università di Napoli'Federico II', Napoli, Italy.
[j] Also at CERN, European Organization for Nuclear Research, Geneva, Switzerland.

https://doi.org/10.1016/j.nima.2025.170467
Received 23 December 2024; Received in revised form 18 March 2025; Accepted 24 March 2025
Available online 1 April 2025
0168-9002/© 2025 The Authors. Published by Elsevier B.V. This is an open access article under the CC BY-NC-ND license (http://creativecommons.org/licenses/by-nc-nd/4.0/).

[11] Department of Physics, Faculty of Science, Ain Shams University, Cairo, Egypt
[12] The British University in Egypt, Cairo, Egypt
[13] Center for High Energy Physics (CHEP-FU), Fayoum University, El-Fayoum, Egypt
[14] Institut de Physique des 2 Infinis de Lyon, Villeurbanne, France
[15] Georgian Technical University, Tbilisi, GA, United States of America
[16] Institute for Research in Fundamental Sciences, Tehran, Iran
[17] INFN Sezione di Bari, Bari, Italy
[18] Università di Bari, Bari, Italy
[19] Politecnico di Bari, Bari, Italy
[20] INFN Laboratori Nazionali di Frascati, Frascati, Italy
[21] INFN Sezione di Napoli, Napoli, Italy
[22] Università di Napoli'Federico II', Napoli, Italy
[23] Dipartimento di Ingegneria Elettrica e delle Tecnologie dell'Informazione - Università Degli Studi di Napoli Federico II, Napoli, Italy
[24] INFN Sezione di Pavia, Pavia, Italy
[25] Università di Pavia, Pavia, Italy
[26] Hanyang University, Seoul, South Korea
[27] Korea University, Seoul, South Korea
[28] Kyung Hee University, Department of Physics, Seoul, South Korea
[29] Sungkyunkwan University, Suwon, South Korea
[30] Benemerita Universidad Autonoma de Puebla, Puebla, Mexico
[31] Centro de Investigacion y de Estudios Avanzados del IPN, Mexico City, Mexico
[32] Universidad Iberoamericana, Mexico City, Mexico
[33] National Centre for Physics, Quaid-I-Azam University, Islamabad, Pakistan
[34] Massachusetts Institute of Technology, Cambridge, MA, United States of America

ARTICLE INFO

Keywords:
Resistive plate chambers
CMS experiment
Gaseous detectors

ABSTRACT

During the so-called Run 3 data taking, the center-of-mass energy for proton–proton collisions at the Large Hadron Collider (LHC) of CERN is 13.6 TeV. The CMS experiment has collected more than 180 fb^{-1} of integrated luminosity for the period of 2022 to 2024. The CMS RPC system faces the challenge of increased LHC instantaneous luminosity up to 2×10^{34} cm^{-2} s^{-1}, providing redundant information for robust muon triggering, reconstruction and identification. To ensure stable data taking, the CMS RPC collaboration has performed a series of detector operation, calibration and performance studies, including the development and maintenance of various software monitoring tools. The detector operation and overall performance at 13.6 TeV, as well as the encountered problems and their corresponding solutions, are documented in this report.

1. Introduction

Four different gaseous detector technologies are used to build up the Muon system [1] of the Compact Muon Solenoid (CMS) experiment [2,3], ensuring its focus on delivering excellent muon triggering and identification, as well as charge and transverse momentum measurement. Drift Tubes (DT), covering pseudorapidity ($|\eta| < 1.2$), are used in the central barrel region, while Cathode Strip Chambers (CSC) ($0.9 < |\eta| < 2.4$) and Gas Electron Multipliers (GEM) ($1.5 < |\eta| < 2.2$) constitute the endcap region. Resistive Plate Chambers (RPC) are used in both regions, covering pseudorapidity up to ($|\eta| < 1.9$), as shown in Fig. 1

With a total number of 1056 double-gap chambers, covering an area of about 3950 m^2, the CMS RPC system is the largest muon detector in the experiment. Each chamber has a copper strips readout plane located between the top and the bottom gaps [1] and consists of 2 gas gaps with 2 mm width each. High-pressure laminate (HPL) with bulk resistivity in the range of $2–5 \times 10^{10}$ Ω cm is used to build each of the detecting gaps, where the High Voltage (HV) is applied to graphite electrodes coated on it. In the barrel, the strips run parallel to the direction of the beam axis and have rectangular shape with a pitch width in the range between 2.28 and 4.10 cm, while in the endcaps, they are trapezoidal with a pitch width between 1.74 and 3.63 cm and run radially to the beam axis direction [3]. In both cases, they measure the phi direction of the particles that pass through them.

To ensure good and stable performance of the chambers, RPCs are operated in avalanche mode at 35%–45% relative humidity with a mixture of 3 pure gases: 95.2% $C_2H_2F_4$, 4.5% iC_4H_{10} and 0.3% SF_6. The latter component is particularly effective in reducing the formation of streamers, while iC_4H_{10} in absorbing the UV photons produced in the recombination process during the formation of the avalanche. The $C_2H_2F_4$ is enhancing the ionization caused by incident particles.

The barrel region of CMS RPC system is divided in the direction along the beam axis into 5 separate wheels (W0, W±1 and W±2), covering the pseudorapidity up to ($|\eta| < 1.2$), while each endcap region has a total number of 4 stations (RE±1, RE±2, RE±3, RE±4), covering the pseudorapidity range ($0.9 < |\eta| < 1.9$) [1]. Each barrel wheel has 12 sectors in azimuthal angle ϕ and 4 stations (RB1, RB2, RB3, RB4), while every endcap station has 36 sectors. Due to requirements in the trigger logic, the chambers are divided into two or three pseudorapidity (η) partitions, called rolls. In most of the barrel detectors, there are two rolls: forward and backward. Only 60 barrel chambers are divided into three rolls, 1 per each azimuthal sector in every wheel (RB2in in W±1 and W0 and RB2out in W±2), called forward, middle and backward (stations RB1 and RB2 have two chambers per sector called IN and OUT, the IN chamber is closer to the center and the OUT chamber is farther away). The endcap RPC detectors are divided into three rolls: A, B, and C, where roll C is the one located towards the center [3–5].

The specific design of the CMS RPC system, as shown in Fig. 1, combined with the well calibrated operating conditions, allows the chambers to cope with high background rates and ensures an excellent time resolution of about 2 ns. It also contributes to the lower absolute number of adjacent fired strips in a single muon hit (called cluster size) of less than 3. These are important parameters that directly impact the assignment of the muon to the correct bunch crossing (BX) (particles in the Large Hadron Collider (LHC) travel in bunches, colliding every 25 ns [6]), ensuring precise and fast muon detection and identification [3].

During the ongoing LHC Run 3 data taking, for the period from 2022 to 2024, the CMS detector recorded ∼180 fb^{-1} and the RPC system contributed very efficiently with its stable performance during the entire period.

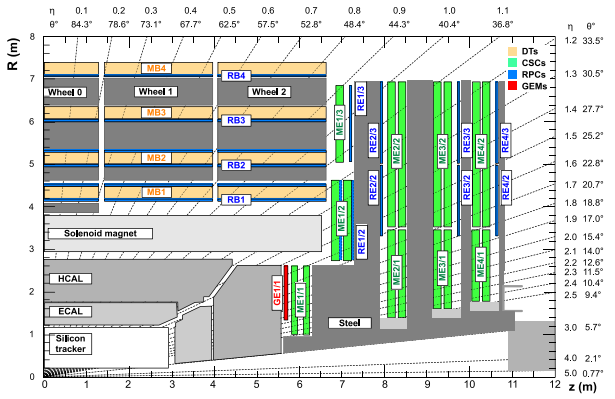

Fig. 1. Schematic view in the r–z plane of a CMS detector quadrant at the start of Run 3 [3].

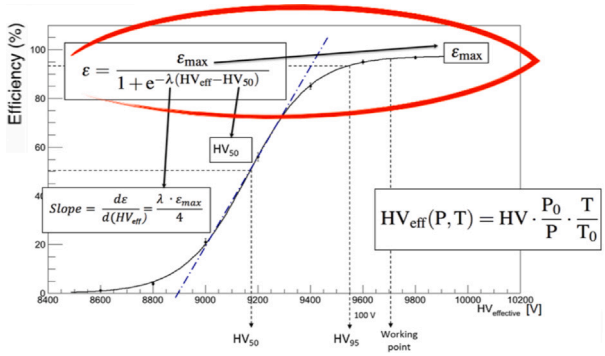

Fig. 2. RPC HV scan Sigmoid fit of the efficiency data points, taken at effective voltage (corrected for pressure variations). The efficiency for every single RPC eta partition (roll) is calculated and fitted for each calibration HV scan run [7].

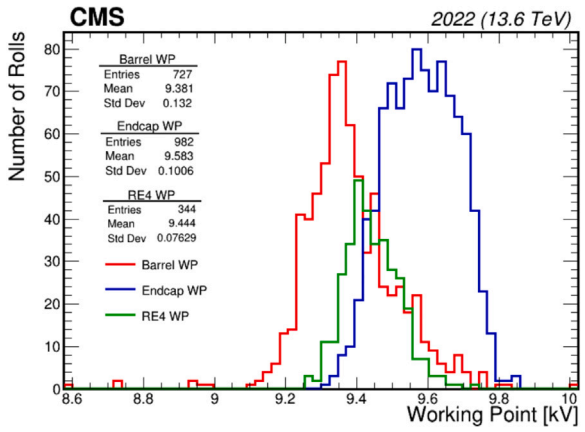

Fig. 3. RPC HV scan Working Point (WP) distribution for 2022 [9].

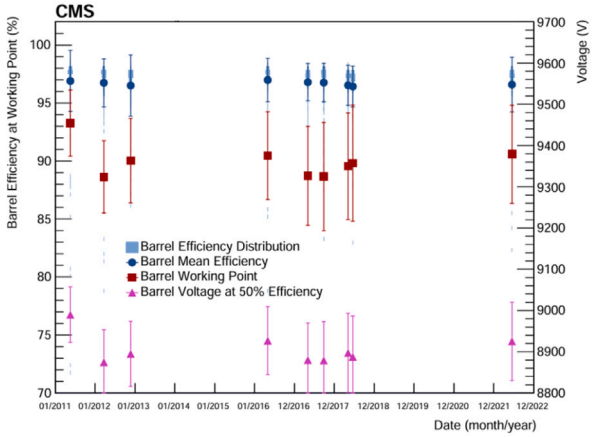

Fig. 4. Temporal evolution of efficiency determined from HV scan data at the WP and the HV at 50% efficiency, for the barrel [9]. In light blue are shown the histograms of the distributions, where the width of the band represents the population of channels having the corresponding efficiency value.

2. CMS RPC operation in Run 3

2.1. RPC calibration

To ensure stable operation of the RPC system during data taking, the high voltage (HV) applied to each chamber is corrected according to environmental conditions. The optimal operating voltage for every chamber, called Working Point (WP), is determined after a series of high voltage scans [7], regularly performed once or twice per year, typically in low and high luminosity conditions.

The HV scan is taken at effective, equidistant voltages within the working range of 8600 to 9800 V. The RPC hit efficiency is obtained using the Segment Extrapolation Method [4], where the RPC efficiency is measured as the ratio between the number of detected and the number of expected hits. To measure this efficiency, aligned hits of DT in the barrel and CSC in the endcaps, called segments, are selected. Hits associated with a segment must belong to a standalone muon track with times corresponding to the time of the RPC readout windows. These segments are then extrapolated to the plane of a given RPC. The detector unit is considered efficient if an RPC reconstructed hit is found within ± 4 strips from the position extrapolated from the DT/CSC segments.

A sigmoid function is used to fit the efficiency data points, taken at effective voltage, as shown in Fig. 2. Here, ϵ_{max}, HV_{eff}, HV_{50} and λ represent the maximum efficiency, the effective high voltage, the voltage at which the fit efficiency is 50% of its maximum value, and the slope of the sigmoid function calculated at HV_{50} [8], respectively. The HV WP is defined as the voltage at 95% efficiency, also known as the Knee (before the plateau) of the efficiency curve, increased of 100 V for barrel and 120 V for endcap [8]. A few differences in the assembly parameters of the chambers (geometry, size, layout, electronics) define the small difference in HV between barrel and endcap detectors [3].

Fig. 3 presents the HV WP distribution for the different parts of the RPC system, as obtained with 2022 data. All sigmoid fits which have failed to fit the data are excluded from the sample, therefore the underflows and the overflows of the distribution are zeros. The clean sample (without the excluded rolls), containing approximately 75% of the rolls, is quite representative. What causes fits to fail may vary between missing extrapolations from other muon detectors and hardware problems like chambers OFF, chambers in single-gap operation mode or rolls with higher number of inactive (masked) electronic channels (strips). In 2024, a new machine learning approach was used to analyze RPC HV scan data with the aim of minimizing the number of failed fits [10].

HV scans of RPCs are also used to study the stability of HV working points over time, as well as the efficiency at WP. Fig. 4 shows the efficiency at WP as a function of time (blue points), the WP (red squares) and the HV at 50% efficiency (magenta triangles) during LHC Run 1 (from 1/2011 to 1/2013), Run 2 (from 1/2016 to 6/2018), and Run 3 (1/2022). Despite the changes in the environmental and luminosity conditions, the different calibrations implemented in the detector allowed the system to keep the efficiency stable.

In addition to all WP validation scans, the good and stable operation and performance of the RPC system is regulated by special HV and

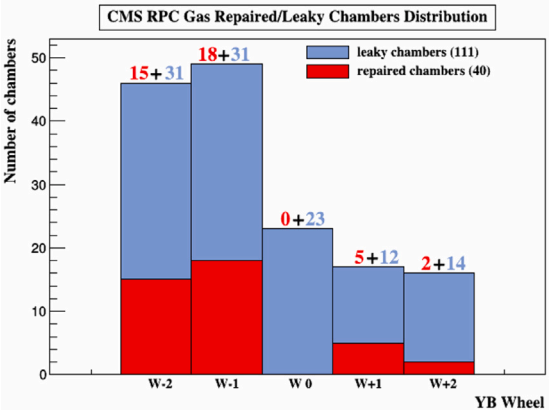

Fig. 5. Distribution of leaking and recovered gas chambers per wheel: the gas status of CMS RPC barrel chambers as of March 2024.

low voltage (LV) maintenance procedures, following regulated access time slots, called technical stops (TS), during the data taking. The HV maintenance aims to identify all problematic channels and parts of the HV power system and fix them in the best feasible way. This allows the recovery of HV lines and change of the detector operation mode from a single-gap to a double-gap one, resulting in better performance of the detectors. The LV maintenance aims to ensure flawless operation along the communication buses, precise functionality of the LV power boards, as well as proper operation and configuration of the on-detector electronics, including the Front-end Boards (FEBs) and the LV distribution boards (LVDB).

2.2. RPC gas system and green-house emission strategy

The standard CMS RPC gas mixture is composed mainly of fluorine composed gases (F-gases) with high global warming potential (GWP) of about 1400. In accordance with CERN wide emission reduction policy, RPCs were obliged to reduce Green House Gases (GHG) emissions. In order to achieve this goal a newly developed "freon (R134a) recuperation system" developed by CERN EP-DT group (Cern gas group) was implemented in Run 3 (2023) [11]. RPC group defined a strategy to reduce overall gas loss of the system by disconnecting the leaking channels (each gas channel provides gas to 2 RPC chambers) in order to have gas in the exhaust and to operate the freon recuperation system in the most efficient way. The freon recovered from the recuperation system was further reinjected into RPC gas system.

The RPC gas system is a 13 m^3 closed-loop volume with re-circulation of 7.3 m^3/h nominal mixture flow: 5 m^3/h for the barrel and 2.3 m^3/h for the endcaps. The increase in the leak rate of the system can be caused by a combination of factors including bad quality components (gas tubes and connectors) and operation (unscheduled gas stops). In addition, switching from freon to Nytrogen (N_2) and back to freon during technical stops, as well as environmental conditions in the experimental cavern, such as humidity and temperature, can accelerate the degradation process of the different components of the system.

The main cause for development of gas leaks in the CMS RPC system are the low-density polyethylene pipes that deteriorate in time becoming brittle or cut due to time aging, as well as the T-shaped or L-shaped polycarbonate gas connectors that break due to stress applied through the gas pipes [3].

The distribution of the gas leak repairs and the number of leaks in all five barrel wheels as of March 2024 is shown in Fig. 5. A total number of 111 gas leaking chambers, caused by cracked or broken pipes are identified in the RPC system barrel region. The number of chambers disconnected from the gas system is 145, of which 110 are leaking gas, while the remaining 35 do not leak gas, but share a gas channel with the gas-leaking chamber. The latter can be recovered and put back into operation if access is available during any of the LHC "End" of the Year Technical Stops (YETS).

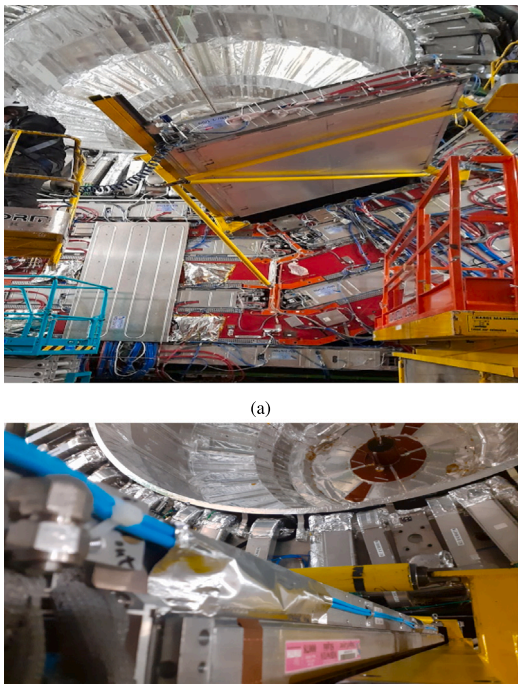

(a)

(b)

Fig. 6. Representation of the new full extraction gas leak reparation protocol: extracted chamber for leak repairs in W−2 during YETS 23/24 (a) and repaired chamber with external (blue) pipes (b).

Following the CMS GHG reduction strategy, about 14% of the RPC system in the barrel has been disconnected. In order to recover this large fraction of disconnected chambers, a new gas leak reparation protocol was validated during the YETS 23/24. A full DT/RPC barrel station (two RPC chambers with a DT chamber in between) was fully extracted, as shown in Fig. 6(a), which allows access for improvement of all weak points, relevant for leak development — replacement of all polyethylene pipes and T-shaped and L-shaped connectors inside the RPC detectors.

During YETS 23/24, two DT/RPC stations in W−2 were fully extracted and all four RPC detectors (2 leaking chambers + 2 connected to them) got new pipes attached outside the chamber and new robust connectors, as shown in Fig. 6(b). The chambers with gas leak were fully recovered and operational during the data taking in 2024.

The already tested procedure of gas leak repair using full extraction is a permanent solution to the gas leak problem in barrel RPC chambers and could be applied thoroughly. No leak is observed in the repaired chambers almost 1 year after reparation. Therefore a massive lifesaving leak repair campaign must be addressed in upcoming YETS or Long Shutdown (LS3) period.

3. CMS RPC performance in Run 3 collisions

LHC Run 3 data taking started with reaching the 13.6 TeV record value of the center-of-mass energy in proton–proton collisions. The CMS experiment started the new data taking period with stable performance, ready to collect good quality data on all possible new phenomena [3].

To validate the RPC system operation after the extensive preparation for Run 3 [12], the CMS RPC system performance has been closely monitored, while a special comparison study on the main RPC detector working parameters has been carried out.

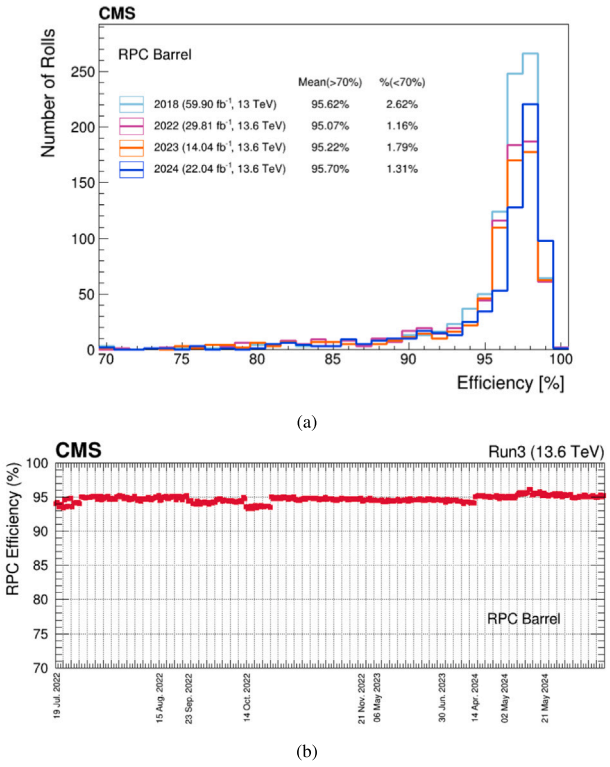

Fig. 7. RPC overall efficiency distribution comparison for the barrel, obtained using 2018, 2022, 2023 and 2024 proton–proton collisions data (a) and RPC barrel average efficiency vs time, obtained using Run 3 proton–proton collisions data (b) [5].

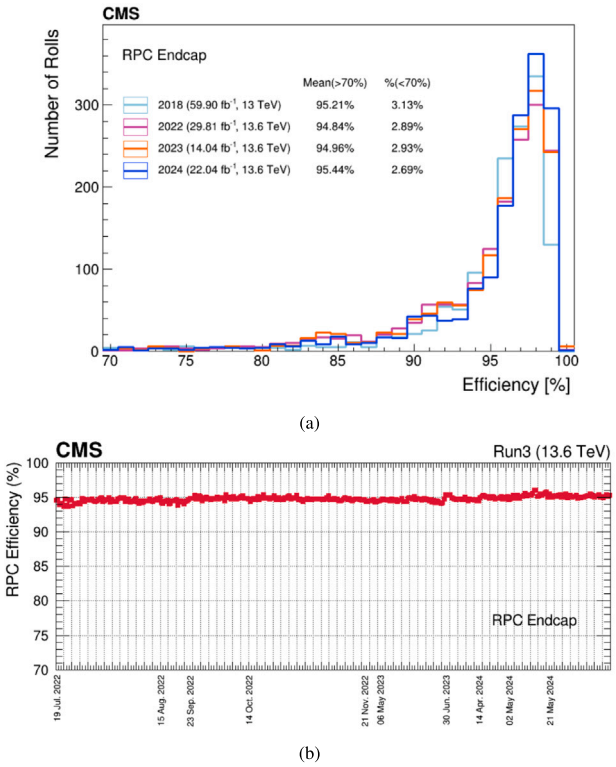

Fig. 8. RPC overall efficiency distribution comparison for the endcap regions, obtained using 2018, 2022, 2023 and 2024 proton–proton collisions data (a) and RPC endcap average efficiency vs time, obtained using Run 3 proton–proton collisions data (b) [5].

The RPC overall efficiency distribution for the barrel and the endcap regions is shown in Fig. 7(a) and 8(a), respectively. The RPC hit efficiency is obtained using the Segment Extrapolation Method [4], described in Section 2.

For correct estimation on the performance of the RPC system configuration during the different years of data taking, all RPC chambers with known hardware problems or switched off due to the CMS gas leak reduction policy are excluded. The underflow entries in the efficiency distributions for both the barrel and the endcap regions are coming from detector units with efficiency lower than 70%, caused by known hardware problems, e.g. chambers working in single gap operation mode. The numbers in the graphs show the average efficiency of good performing RPC units, as well as the fraction of problematic ones.

Fig. 7(b) and Fig. 8(b) show the RPC efficiency history for the barrel and endcap regions respectively. The drops in the efficiency, appearing for different periods in time, are due to known hardware problems, which were successfully fixed.

Comparing the efficiency of the RPC system with previous measurements and CMS requirements to maintain efficiency at the 95% level [1], the RPC efficiency measured in Run 3 (up to 2024) is stable and in accordance with expectations. The stable fraction of detector units operating at lower efficiency (shown in Figs. 7(a) and 8(a)) demonstrates the success of the HV, LV and gas system maintenance during the data taking period.

Another important RPC working parameter, which affects the RPC spacial resolution, is the cluster size — number of adjacent fired strips in a single muon hit. One of the most important prerequisites for the correct functioning of the RPC system is the stability of the cluster size over time, which also guarantees the stability of the system. The comparison of the cluster size distribution of RPC hits associated with muons in the barrel and the endcap are shown in Fig. 9(a) and Fig. 10(a), respectively, while the average cluster size history is presented in Fig. 9(b) for the barrel and Fig. 10(b) for the endcap regions.

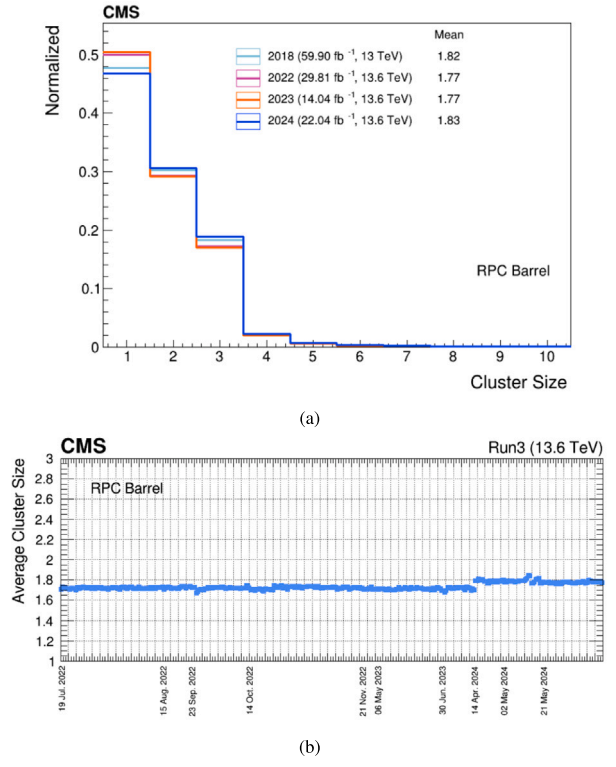

Fig. 9. RPC cluster size distribution comparison for the barrel, obtained using 2018, 2022, 2023 and 2024 proton–proton collisions data (a) and RPC barrel average cluster size vs time, obtained using Run 3 proton–proton collisions data (b) [5].

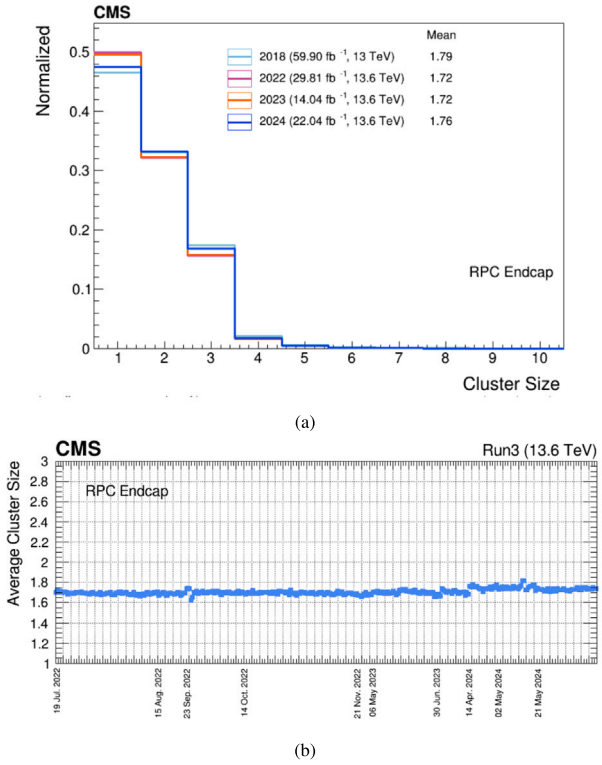

Fig. 10. RPC cluster size distribution comparison for the endcap regions, obtained using 2018, 2022, 2023 and 2024 proton–proton collisions data (a) and RPC endcap average cluster size vs time, obtained using Run 3 proton–proton collisions data (b) [5].

Even though, with respect to the distance to the beam pipe, the RPC readout strips pitch width varies from 1.7 cm in the innermost stations to 4.1 cm for the outermost stations [3], resulting in possible larger cluster size number for the different detector parts, the RPC system mean cluster size measured in Run 3 is below 2, which is comparable and in agreement with the expectations.

4. Conclusion

The CMS RPC system kept its stable performance during the ongoing Run 3 data taking. The RPC group performed a series of calibration studies and scans on the HV working parameters, gas leaks and LV to ensure the optimal operation conditions.

Following the CMS experiment aim to minimize the environmental impact of the RPC operational gas mixture, a new policy to disconnect all leaking chambers from the gas distribution was established. This allowed the successful validation and calibration of the new freon recuperation system.

In addition, a new gas leak reparation procedure was successfully tested and validated at the CMS experiment site to keep the number of gas disconnected detectors to a minimum and ensure the repaired chambers are fully operational with no side effects from the reparation and no observed gas leak.

The results from the Run3 data analysis show stable performance of the RPC system, with average efficiency of $\sim 95\%$ and average cluster size below 2. Results obtained from the Run 3 data analysis confirm the success and importance of all calibration activities performed during the data taking period, resulting in the RPC system optimal and smooth operation.

Declaration of competing interest

The authors declare that they have no known competing financial interests or personal relationships that could have appeared to influence the work reported in this paper.

Acknowledgments

We congratulate our colleagues in the CERN accelerator departments for the excellent performance of the LHC and thank the technical and administrative staffs at CERN and at other CMS institutes for their contributions to the success of the CMS effort. In addition, we gratefully acknowledge the computing centres and personnel of the Worldwide LHC Computing Grid and other centres for delivering so effectively the computing infrastructure essential to our analyses. Finally, we acknowledge the enduring support for the construction and operation of the LHC, the CMS detector, and the supporting computing infrastructure provided by the following funding agencies: FWO (Belgium); CNPq, CAPES and FAPERJ (Brazil); MES and BNSF (Bulgaria); CERN, Switzerland; CAS, MoST, and NSFC (China); MINCIENCIAS (Colombia); CEA and CNRS/IN2P3 (France); SRNSFG (Georgia); IPM (Iran); INFN (Italy); MSIP and NRF (Republic of Korea); BUAP, CINVESTAV, CONACYT, LNS, SEP, and UASLP-FAI (Mexico); PAEC (Pakistan); DOE and NSF (USA).

References

[1] CMS Collaboration, The CMS muon project: Technical Design Report, CERN, Geneva, 1997, URL https://cds.cern.ch/record/343814.
[2] CMS Collaboration, The CMS Experiment at the CERN LHC, JINST 3 (2008) S08004, http://dx.doi.org/10.1088/1748-0221/3/08/S08004.
[3] CMS Collaboration, Development of the CMS detector for the CERN LHC Run 3, JINST 19 (2024) P05064, http://dx.doi.org/10.1088/1748-0221/19/05/P05064.
[4] CMS Collaboration, Performance study of the CMS barrel resistive plate chambers with cosmic rays, JINST 5 (2010) T03017, http://dx.doi.org/10.1088/1748-0221/5/03/T03017.
[5] CMS Collaboration, RPC performance with early 2024 data, Tech. Rep., CERN, 2024, URL https://cds.cern.ch/record/2908774.
[6] P. Evans, J. Bryant, LHC Collaboration Collaboration, The CERN large hadron collider: Accelerator and experiments, JINST 3 (2008) S08001, http://dx.doi.org/10.1088/1748-0221/3/08/S08001.
[7] M. Abbrescia, et al., CMS Collaboration, Cosmic ray tests of double-gap resistive plate chambers for the CMS experiment, Nucl. Instruments Methods Phys. Res. Sect. A: Accel. Spectrometers, Detect. Assoc. Equip. 550 (2005) 116–126, http://dx.doi.org/10.1016/j.nima.2005.06.074.
[8] M. Shah, et al., CMS Collaboration, The CMS RPC detector performance and stability during LHC RUN-2, JINST 14 (2019) C11012, http://dx.doi.org/10.1088/1748-0221/14/11/C11012.
[9] CMS Collaboration, 2022 High Voltage Scan studies for RPC, CERN, 2024, URL https://cds.cern.ch/record/2916745.
[10] CMS Collaboration, Machine Learning approach to CMS RPC HV scan data analysis, CERN, Geneva, 2024, URL https://cds.cern.ch/record/2916751.
[11] M.C. Arena, R. Guida, B. Mandelli, G. Rigoletti, Recuperation systems for fluorinated gases at the CERN LHC Experiments, Nucl. Instruments Methods Phys. Res. Sect. A: Accel. Spectrometers, Detect. Assoc. Equip. 1068 (2024) 169789, http://dx.doi.org/10.1088/1748-0221/15/10/C10025.
[12] M. Shopova, et al., CMS Collaboration, The CMS RPC system readiness for LHC Run-3 data taking, Nucl. Instruments Methods Phys. Res. Sect. A: Accel. Spectrometers, Detect. Assoc. Equip. 1052 (2023) 168272, http://dx.doi.org/10.1016/j.nima.2023.168272.